# NUMERICAL SIMULATIONS OF SELF-SUSTAINED AEROELASTIC OSCILLATIONS AT LOW REYNOLDS NUMBERS

**Weixing Yuan*, Baoyuan Wang**, Dominique Poirel****
***National Research Council Canada, ****Royal Military College of Canada**
*Weixing.yuan@nrc-cnrc.gc.ca;baoyuan.wang@nrc-cnrc.gc.ca;poirel-d@rmc.ca*

**Keywords**: *Fluid-structure interaction, limit-cycle oscillation, aeroelasticity, low-Re aerodynamics, UAV aerodynamics*

## Abstract

*By coupling a two-degree-of-freedom structural model with an in-house incompressible code, numerical simulations were performed for a NACA 0012 airfoil undergoing self-sustained oscillations. As observed in experiments, the numerical simulations confirmed the presence of the pitch-heave limit-cycle oscillations of the airfoil at transitional Reynolds numbers, as a result of the nonlinear low-Re aerodynamics. The computed results revealed that the pitch motion of the pitch-heave limit-cycle oscillations at $Re_c < 80{,}000$ was mainly maintained by the pitching moment feeding energy from the flow to the airfoil, while the pitch motion is believed to be sustained through the coupling with the second degree of freedom in heave at $Re_c > 80{,}000$. Both pitch and heave motions were bounded by the pitching moment at ultimate pitch angles to a limit-cycle oscillation.*

## 1 Introduction

In the range of Reynolds numbers $10^4 \le \mathrm{Re} \le 10^6$, where emerging unmanned air vehicles (UAVs) usually fly, complex viscous flow phenomena can occur, such as laminar boundary layer separation, transition of the laminar shear layer, and subsequent turbulent re-attachment, leading to the formation of a laminar separation bubble (LSB). Although self-excited low-amplitude oscillations of free-to-rotate airfoils or wings at transitional Reynolds numbers were observed in 1950s [1] [2], there are few further studies reported on this topic. Recent experimental aeroelastic investigations carried out at the Royal Military College of Canada (RMC) on a NACA 0012 airfoil confirmed self-sustained oscillations of the airfoil in the case where the airfoil was mounted on a support so as to permit a free rotation with and without vertical heave [3] [4]. The investigations concluded that the trailing-edge laminar separation played a significant role in the airfoil oscillations [3] [5]. In order to obtain a deeper insight into the physics of low-Re limit-cycle oscillations (LCOs) and their probable impact on UAVs, the National Research Council Canada (NRC) and RMC are performing aeroelastic calculations for flows past airfoils oscillating at a free-to-rotate-and-heave motion condition. This work is supported by the Department of National Defence (DND) Technology Investment Fund (TIF). The preliminary results of one-degree-of-freedom (1DOF) free-to-rotate (pitch only) and 2DOF free-to-rotate-and-heave (pitch-heave) airfoils were presented in Ref. [6]. This paper reports further investigations in terms of Reynolds number effects on the 2DOF LCOs.

## 2 Numerical Methods

The NRC in-house code INSflow, developed to compute three-dimensional (3D) unsteady incompressible flows, was applied in this study. INSflow has been used for a number of large-eddy simulations (LES) and unsteady Reynolds-averaged Navier-Stokes (URANS) calculations for various flows in incompressible regimes.

INSflow applies the integral form of the conservation laws of mass and momentum. A fully-implicit, second-order temporal differencing scheme was implemented in the discretization. The discretization of the convective and diffusive fluxes was carried out in a co-located variable arrangement using a finite-volume approach that was second-order accurate in space. The coupling of the pressure and velocity was handled using a modified SIMPLE algorithm. The calculations were performed on moving grids; the velocity of the grid movement was included in the governing equations in an inertial frame of reference. In order to avoid artificial mass sources generated by the grid velocity, a space conservation law was introduced to ensure a fully conservative property in the computations.

A linear 2DOF rigid-body structural model was assumed for the rig, leading to the following equations of motion for the aeroelastic system:

$$I_{EA}\ddot{\theta} - 0.5M_{\theta}cx_{\theta}\ddot{h} + D_{\theta}\dot{\theta} + K_{\theta}\theta = M_{EA}(t), \quad (1)$$

$$M_h\ddot{h} - 0.5M_{\theta}cx_{\theta}\ddot{\theta} + D_h\dot{h} + K_h h = L(t). \quad (2)$$

The right hand sides of the equations represent the aerodynamic moment and lift, respectively. In the equations, $\theta$ is the pitch angle, $h$ is the heave (plunge) displacement, $I_\theta$ is the mass moment of inertia about the elastic axis (EA), $c$ is the airfoil chord length, and $x_\theta$ is the distance from the elastic axis to the center of gravity normalized by the half chord length. $M_h$ and $M_\theta$ are the masses, $D_h$ and $D_\theta$ are the structural damping coefficients, and $K_h$ and $K_\theta$ are the structural stiffness coefficients, in heave and pitch, respectively. The structural equations were discretized in a fully-implicit manner with second-order accuracy in time:

$$\dot{\theta}^{n+1} = \frac{3\theta^{n+1} - 4\theta^{n} + \theta^{n-1}}{2\Delta t} + O(\Delta t^2), \quad (3)$$

$$\ddot{\theta}^{n+1} = \frac{3\dot{\theta}^{n+1} - 4\dot{\theta}^{n} + \dot{\theta}^{n-1}}{2\Delta t} + O(\Delta t^2) = \frac{9\theta^{n+1} - 24\theta^{n} + 22\theta^{n-1} - 8\theta^{n-2} + \theta^{n-3}}{4\Delta t^2} + O(\Delta t^2), \quad (4)$$

where the superscript $(n+1)$ represents the new time level.

## 3 Computed Results and Discussion

### 3.1 Setup

In the nominal configuration, the masses of all moving parts and that of the pitching part only were $M_h = 2.5$ kg and $M_\theta = 0.77$ kg, respectively. The mass moment of inertia about the elastic axis located at 18.6% of the chord length from the leading edge was $I_\theta = 0.00135$ kg·m$^2$ and the structural stiffnesses as dictated by the springs were $K_h$ = 1484 N/m and $K_\theta$ = 0.30 N·m for the two types of motion, respectively. The structural damping properties were represented by the classical linear viscous model, $D_h$ = 10 N·s/m and $D_\theta$ = 0.002 N·m·s. The static imbalance, non-dimensional distance (by half-chord) from the elastic axis to the center of gravity was $x_\theta = 0.19$.

As in the experiments, a NACA 0012 airfoil was chosen as the test case. The airfoil had a chord length of $c$ = 0.156 m. The freestream velocity of the nominal test case was specified as $U_\infty = 7.5$ m/s, resulting in $\mathrm{Re_c}$ = 77,000. To investigate the Reynolds number effects, an additional test case at $U_\infty = 8.25$ m/s, i.e., $\mathrm{Re_c}$ = 85,000, was conducted. 3D LES-based calculations were carried out on an O-H-type mesh with 481×97×33 grid points. The span was set to 0.2$c$. The farfield boundaries were located at about 10 chords away from the surface of the airfoil. On the O-type meshes of the 2D sections, the airfoil had a blunt trailing edge. The inner part of the O-type mesh pitched rigidly, in unison with the airfoil, while the outer part remained non-rotating. The mesh layer between the inner and outer parts was dynamic, rather than sliding, and deformed during the airfoil pitching motion. This functioned satisfactorily as long as the deformations remained small. The use of the non-rotating mesh for the outer part eased the implementation of the farfield boundary conditions. No-slip boundary conditions were used for the surfaces of the rectangular wing

and periodic boundary conditions were applied in the spanwise direction. Initial conditions, for both the fluid and elastic equations, are needed to perform the calculations. The nominal 2DOF simulations at $Re_c$ = 77k were started from a set of the instantaneous 1DOF results presented in Ref. [6], whereas the simulations of $Re_c$ = 85k were started from a set of the instantaneous results of the $Re_c$ = 77k case.

### 3.2 2DOF Pitch-heave LCOs at $Re_c$ = 77k

The nominal 2DOF pitch-heave test case at $Re_c$ = 77k presented in Ref. [6] was further investigated. Figure 1 shows the computed pitch angle and heave response of the 2DOF pitch-heave NACA 0012 airfoil compared with experimental data. As shown in the plots, the predicted LCO frequency and averaged pitch angle and heave amplitudes were 2.97 Hz, 5.75° and 1.36 mm. The computed results compared reasonably well to the experimental data at $Re_c$ = 77k: 3.1 Hz, 5.6° and 1.1 mm, respectively. Note that the time of the simulation results is normalized by the experimental LCO period.

Figure 2 shows the computed aerodynamic coefficients of the 2DOF pitch-heave airfoil as a function of pitch angle and heave displacement, respectively. The lift coefficient as a function of pitch angle (left plot) and heave (right plot), respectively, showed unsteady but nearly linear effects. Slight nonlinearity appeared at $\theta \approx \pm 2.5°$. In contrast, the pitching moment as a function of pitch angle showed apparent nonlinearity, in particular at around zero pitch. Note that, throughout the paper, the pitching moment is always expressed about the elastic axis. Similar to the 1DOF LCO, the aerodynamic pitching moment coefficient as a function of pitch angle, during one pitch cycle, confirmed the clockwise loop, indicating positive work done by the flow at the center position near 0° pitch angles. Also, the loop of the lift coefficient as a function of heave displacement was clockwise, confirming positive work done by the lift force. This resulted from the positive lift coefficient at zero heave displacement when the airfoil heaved upwards as mentioned above, meaning that the lift force fed energy to the airfoil sustaining the limit-cycle oscillations in heave. The predicted work per cycle done by the aerodynamic pitching moment and lift force was $0.30\times10^{-3}$ Nm and $1.9\times10^{-3}$ Nm, which compared well with the experiments at Re = 77k: $0.28\times10^{-3}$ Nm and $1.4\times10^{-3}$ Nm, respectively.

Figure 3 shows the instantaneous flowfields of the 2DOF NACA 0012 airfoil obtained from the computations. Similar to the 1DOF case presented in Ref. [6], laminar boundary layer separation and laminar-turbulent transition can be clearly seen, e.g., in Figure 3a and Figure 3b. The flattened pressure plateaus indicate the flow separation owing to the adverse pressure gradient. At $\theta \approx 0°$ when the airfoil was pitching up (Figure 3a), separated flow was observed on the upper surface near the trailing edge because the laminar separation occurred too close to the trailing edge to allow for the flow to transition to turbulence and reattach to the surface. This happens usually at low angles of attack due to low-Re aerodynamics at static conditions (cf. Ref. [7]). Note that the skin friction coefficient was defined positive parallel to the airfoil surface, rather than the x-direction. Since the negative x-component of the velocity in the separation zone, on the upper surface near the trailing edge at $\theta \approx 0°$, was small compared to the y-component, the skin friction coefficient was not negative but close to zero. Elsewhere, laminar-turbulent transition or a laminar separation bubble (if phase averaged) was observed. The transition process was evidenced by the vortex shedding from the primary separated shear layer and rolling up on the lower surface at $\theta \approx 0°$ when the airfoil was pitching up and on the upper surface at $\theta \approx 5.75°$, see spanwise vorticity distributions in Figure 3a (red color) and Figure 3b (blue color), respectively. In the case with a transitional separation bubble, the pressure plateau terminated when the transition of the separated shear layer caused a rapid increase in the surface pressure as shown by the dashed line in Figure 3a for the lower surface at $\theta \approx 0°$ when pitching up and the solid line in Figure 3b-f for the upper surface when pitching down.

The snapshots shown in Figure 3 were extracted from an oscillation cycle of the 3D LES. They represent flowfields at critical time instants of a limit-cycle oscillation. Starting from Figure 3a, where the airfoil was pitching up through the center position at zero degrees, the flow separation (bubble, if phase averaged) on the lower surface caused noticeable suction, resulting in a nose-up pitching moment, and thus contributing to the pitch-up rotation. During the pitch-up motion, the angle of attack of the airfoil increased and the separation on the upper surface moved upstream according to the low-Re aerodynamic behavior at static conditions. Subsequently, the nose-down pitching moment, mainly caused by the pressure suction on the airfoil upper surface, reached its maximum near the maximum pitch angle (plot b). This nose-down pitching moment forced a pitch-down rotation (plots c-h) and thus bounded the pitching motion to a limit-cycle oscillation. Because of the time delay, the upstream movement of the separation on the upper surface continued to about 3° (plot c). At this time instant, the separation on the upper surface started moving downstream (plot d), which was consistent with the low-Re aerodynamics at static conditions. The downstream movement of the separation increased the pitching arm and thus retained a nose-down pitching moment. This separation movement continued from 3° (plot c) to about -3° (plot g). In accordance with the low-Re aerodynamic behavior at static conditions, the separation point on the lower surface moved upstream as well when the nose-down angle increased (plots e-g). Owing to the upstream movement of the separation point on the lower surface and the downstream movement of the separation point on the upper surface, the separation zones were comparable on both sides and the pitching moment changed sign from nose down to nose up at about -2.7° (plot g). The pitch-down rotation continued until the positive (nose-up) pitching moment reached its maximum near -5.75° (plot h), leading to a subsequent pitch-up rotation (plot i).

As mentioned earlier, the lift coefficient was nearly linear with the pitch angle, with a slight but tangible nonlinearity at about ±2.5°. Driven by the increasing lift force, the airfoil heaved up during the period from Figure 3a to Figure 3b. At the maximum pitch angle (Figure 3b), the inertial effect of the pitching part through the second derivative of the pitch angle reached a maximum and thus bounded the heave motion to a limit-cycle oscillation, cf. Eq. 2.

### 3.3 2DOF Pitch-heave LCOs at $Re_c$ = 85k

During the experimental studies, Poirel and Mendes observed a peculiar behavior of the particular structural configuration [4]: the LCO amplitudes exhibited a sudden increase for $Re_c$ > 80k and an apparent change of regime delineated by a boundary at $Re_c$ = 80k for the frequency. This change of regime was also observed for the 1DOF case as reported in Ref. [3]. To gain deeper insights into the flow physics and its correlations with the experimentally observed LCO behavior change, numerical simulations were performed for a higher Reynolds number test case, i.e., $U_\infty$ = 8.25 m/s and $Re_c$ = 85k. The simulations were started from a set of instantaneous solutions of the earlier case at $Re_c$ = 77k.

Figure 4 shows the computed pitch angle and heave response of the 2DOF pitch-heave NACA 0012 airfoil at $Re_c$ = 85k. As shown in the figure, the LCO converged to noticeably higher amplitude for both pitch angle and heave displacement. By superimposing the numerical results upon the experimental data, Figure 5 confirms the trend of the LCO amplitude increase with the increasing Reynolds number. The slight discrepancy between the numerical and experimental results might be attributed to the slightly different setups, since both the freestream turbulence intensity (0.2%) and the possible structural non-linearity in the experiments were not considered in the current numerical study.

The computed aerodynamic coefficients of the 2DOF NACA 0012 airfoil at $Re_c$ = 85k as a function of pitch angle and heave displacement are shown in Figure 6. Except for larger magnitudes of the lift coefficients and the LCO amplitudes when compared with the case at $Re_c$ = 77k, the lift coefficients at $Re_c$ = 85k

showed quasi-linear variations with the pitch angle and heave displacement, without any noticeable nonlinearity at low angles. However, noticeable change can be seen for the pitching moment coefficients as a function of the pitch angle. Not only was the pitching moment magnitude around zero degrees smaller, but also the loop changed direction. The counter-clockwise loop resulted in a negative value of the work done by the pitching moment, as listed in Table 1. The negative work indicates that the airfoil fed energy to the flow through pitching motion at $Re_c$ = 85k, which was completely different from the case at $Re_c$ = 77k, where the flow transfered energy to the airfoil. Based on these observations, we come to the argument that the pitch motion was mainly maintained by the heave motion at $Re_c$ > 80k.

The quasi-linearity of the lift coefficient with the pitch angle and the heave displacement is plotted in another view as a function of time in Figure 7. Phase shifts were observed: the heave displacement lagged the lift coefficient and the latter lagged the pitch angle. This implied the dependence of the heave displacement on the lift coefficient and the latter on the pitch angle. This dependence or correlation was the same for both Reynolds numbers. However, the nonlinear pitching moment coefficients showed different phase shifts with the pitch angles at the two Reynolds numbers. As shown in Figure 7, at zero pitch angles, the pitching moment lagged the pitch angle at $Re_c$ = 77k, while it was the reverse at $Re_c$ = 85k.

The flowfield at $Re_c$ = 85k is depicted in Figure 8, which looks comparable to that at $Re_c$ = 77k shown in Figure 3. However, closer comparisons confirmed that in general, the laminar-turbulent transition occurred earlier at $Re_c$ = 85k and possibly the correlated laminar separation too. For quantitative comparison purposes, the inception locations of the laminar separation bubble are explicitly listed in Table 2. The flow separated earlier at higher angles at $Re_c$ = 85k when compared with $Re_c$ = 77k, which is consistent with the low-Re aerodynamics at static conditions, because the pitching amplitude was higher at $Re_c$ = 85k. Related to the earlier separation shown in Figure 8b-c, the suction peak on the upper surface at the leading edge was much higher when the airfoil was heaving up at $Re_c$ = 85k than that at $Re_c$ = 77k. It reached $Cp$ = -1.7 at the ultimate pitch angle at $Re_c$ = 85k. This resulted in higher lift force and thus led to higher amplitude of the heave displacement. On the other hand, at low angles, i.e., at zero degrees, although the separation did not occur earlier at $Re_c$ = 85k, earlier flow transition was observed on the lower surface, cf. Figure 8a vs. Figure 3a. The earlier flow transition resulted in shorter separation bubble and shorter pitching arm as well. This explained the occurrence of the small negative pitching moment at zero pitch angles for $Re_c$ < 85k and the counter-clockwise loop of the pitching moment – pitch angle chart, see Figure 6. Although the pitching moment was negative at zero degrees for $Re_c$ < 85k when the airfoil was pitching up, the strong contribution from the heave motion, as expressed by the inertial term of the pitching part through the second derivative of the heave displacement in Eq. 1, transferred energy to the airfoil, sustaining the oscillations in pitch.

## 4 Conclusions

Numerical simulations were performed for a NACA 0012 airfoil in 2DOF pitch-heave limit-cycle oscillations at transitional Reynolds numbers. The predicted LCO frequency and amplitude were in good agreement with the experimental observations.

The simulations have confirmed the Reynolds number effects observed in the experiments – the LCO amplitude increased with increasing Reynolds number beyond $Re_c$ = 80k. In particular, the aerodynamic pitching moment did positive work on the airfoil for $Re_c$ < 80k, maintaining the pitch motion of the LCO, while the work was negative for $Re_c$ > 80k, and therefore, the pitch oscillation was sustained through the coupling mechanism with heave motion transferring energy from the flow to the airfoil.

## References


[1] van de Vooren I A I and Bergh H. *Spontaneous Oscillations of an Aerofoil due to Instability of the Laminar Boundary Layer*, Report F. 96, National Luchtvaart Laboratorium, 1951.

[2] Lambourne N C. *An Experimental Investigation on the Flutter Characteristics of a Model Flying Wing, Technical Report*, No. 2626, Aeronautical Research Council, 1952.

[3] Poirel D, Harris Y and Benaissa A. Self-sustained Aeroelastic Oscillations of a NACA 0012 Airfoil at Low-to-moderate Reynolds Numbers. *Journal of Fluids and Structures*, Vol. 24, No. 5, pp700-719, 2008.

[4] Poirel D and Mendes F. Experimental Investigation of Small Amplitude Self-sustained Pitch-plunge Oscillations of a NACA0012 Airfoil at Transitional Reynolds Numbers. *50th AIAA Aerospace Sciences Meeting*, Nashville, Tennessee, AIAA 2012-0040, 2012.

[5] Poirel D and Yuan W. Aerodynamics of Laminar Separation Flutter at a Transitional Reynolds Number. *Journal of Fluids and Structures*, Vol. 26, No. 7-8, pp 1174–1194, 2010.

[6] Yuan W, Poirel D and Wang B. Simulations of Airfoil Limit-cycle Oscillations at Transitional Reynolds Numbers. *50th AIAA Aerospace Sciences Meeting*, Nashville, Tennessee, AIAA 2012-0041, 2012.

[7] Huang R-F and Lin C. Vortex Shedding and Shear-Layer Instability of Wing at Low-Reynolds Numbers. *AIAA Journal*, Vol. 33, No. 8, pp1398-1403, 1995.


## Copyright Statement



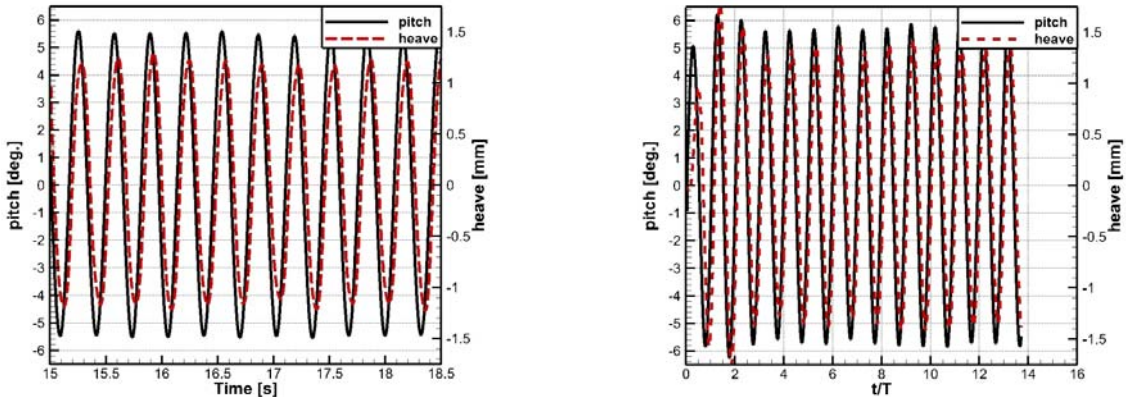


Figure 1. Pitch angle and heave response of the 2DOF pitch-heave NACA 0012 airfoil at $U_\infty$ = 7.5 m/s, $Re_c$ = 77,000. Left: experimental; right: numerical; T is the experimental LCO period.

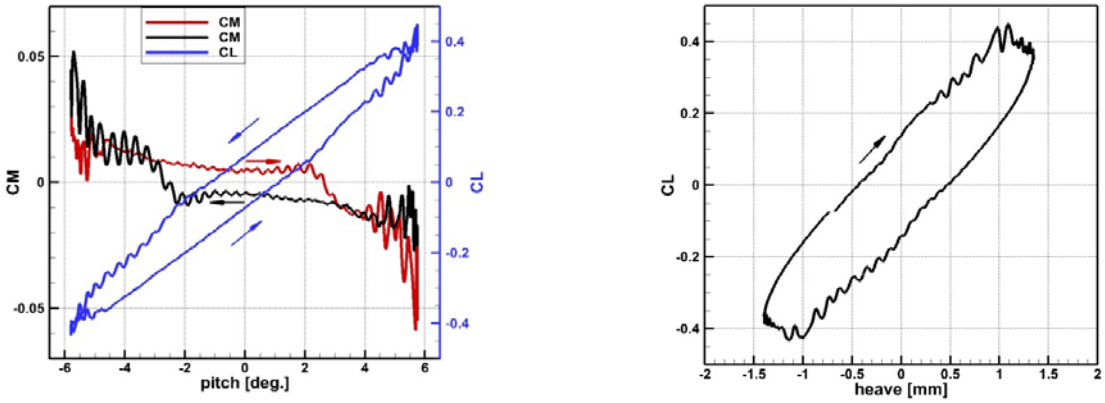


Figure 2. Computed phase-averaged aerodynamic coefficients of the 2DOF pitch-heave NACA 0012 airfoil as a function of pitch angle and heave displacement during one LCO cycle at $U_\infty$ = 7.5 m/s, $Re_c$ = 77,000.

a)
θ = 0.33°
pitch up
h=-0.81mm
heave up

b)
θ = 5.88°
~ max pitch
h=1.18mm
heave up

c)
θ=3.07°
pitch down
h=1.27mm
~ max heave

d)
θ=1.71°
pitch down
h=1.05mm
heave down

e)
θ = 0.23°
pitch down
h=0.76mm
heave down

f)
θ =-1.98°
pitch down
h=0.24mm
heave down

g)
θ =-2.70°
pitch down
h=0.05mm
heave down

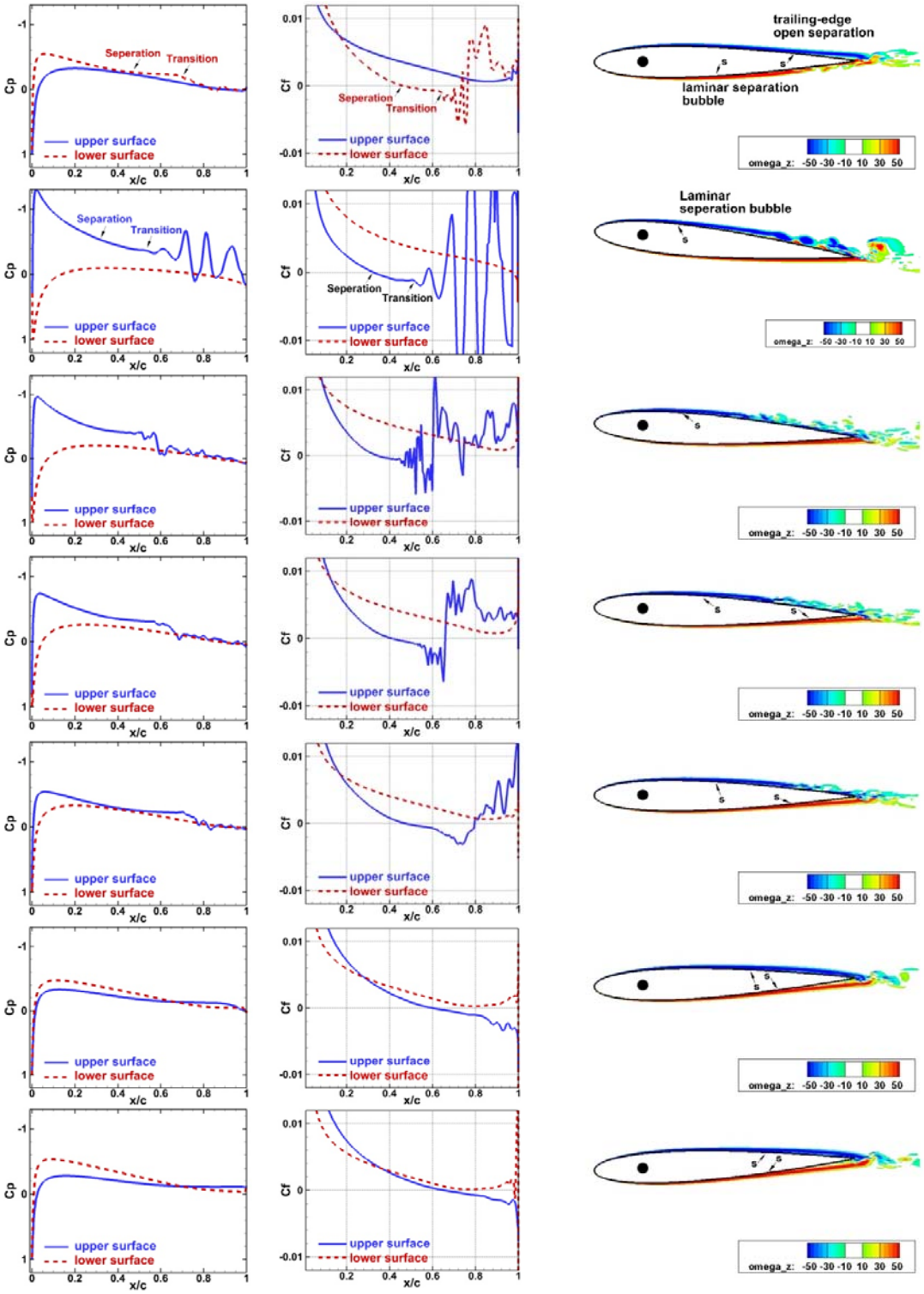


Figure 3. 3D LES computed instantaneous surface pressure coefficients, friction coefficients and non-dimensional spanwise vorticity ( $\omega_z$ ) distributions on the mid-span of the 2DOF pitch-heave NACA 0012 wing during one LCO cycle at $U_\infty$ = 7.5 m/s, $Re_c$ = 77,000. Continued on next page.

h)
θ =-5.84°
~ max pitch
h=-1.20mm
heave down

i)
θ = 0.08°
pitch up
h=-0.71mm
heave up

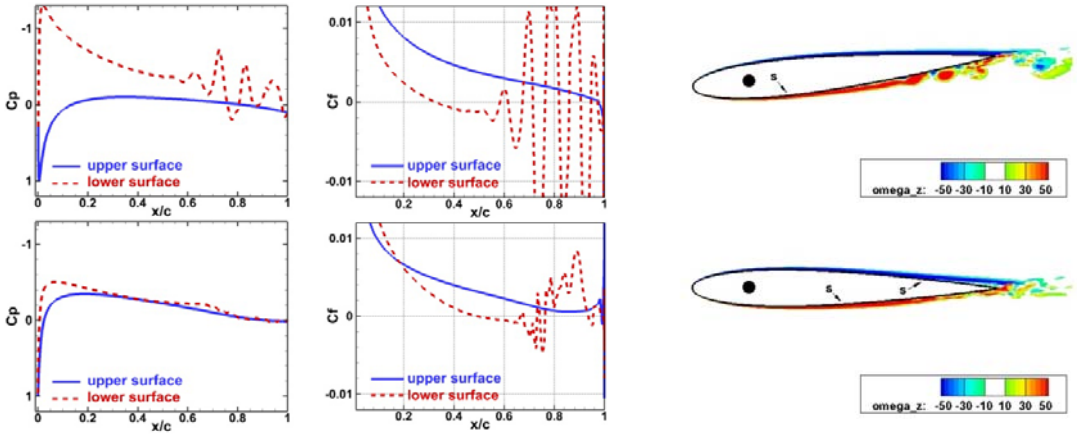


Figure 3. For caption see previous page.

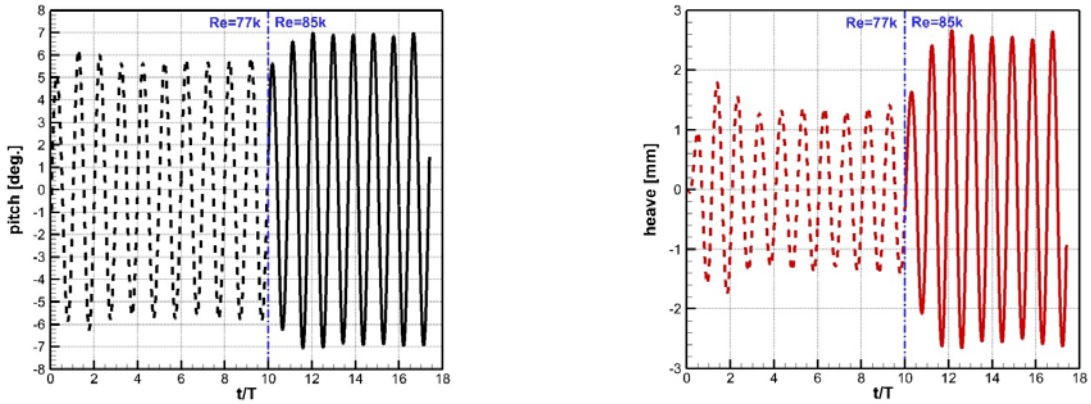


Figure 4. Pitch angle and heave response of the 2DOF pitch-heave NACA 0012 airfoil at $U_\infty$ = 8.25 m/s, $Re_c$ = 85,000.

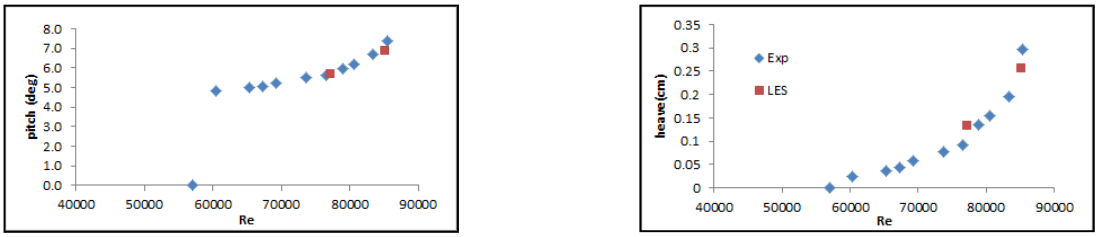


Figure 5. Pitch angle and heave response of the 2DOF pitch-heave NACA 0012 airfoil as a function of Reynolds number.

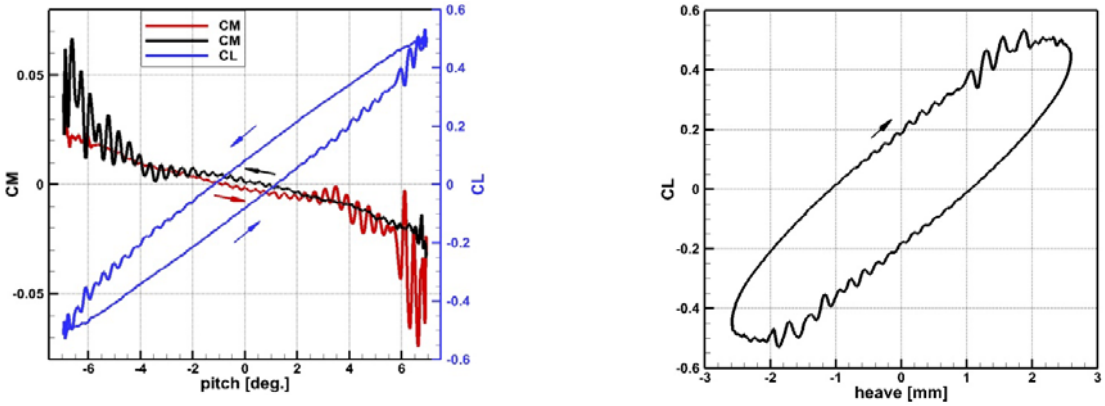


Figure 6. Computed phase-averaged aerodynamic coefficients of the 2DOF pitch-heave NACA 0012 airfoil as a function of pitch angle and heave displacement during one LCO cycle at $U_\infty$ = 8.25 m/s, $Re_c$ = 85,000.

Table 1 Overall characteristics of the 2DOF pitch-heave oscillations

| Cases | Cycles | Pitch peaks (°) | Heave peaks (mm) | Frequency (Hz) | Work by moment ($10^{-3}$ Nm) | Work by lift ($10^{-3}$ Nm) |
|---|---|---|---|---|---|---|
| Re = 77k | ≥12 | 5.75 | 1.36 | 2.97 | 0.30 | 1.9 |
| Re = 85k | ≥6 | 6.95 | 2.59 | 3.14 | -0.58 | 5.5 |

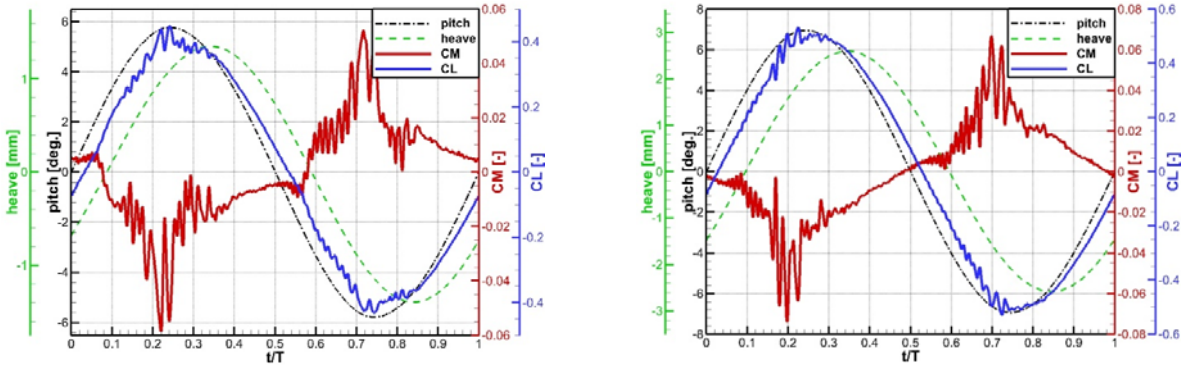


Figure 7. Computed phase-averaged pitch angle and heave response and aerodynamic coefficients of the 2DOF pitch-heave NACA 0012 airfoil as a function of time during one LCO cycle. Left: $U_\infty$ = 7.5 m/s, $Re_c$ = 77,000; right: $U_\infty$ = 8.25 m/s, $Re_c$ = 85,000.

Table 2 Separation inception location (x/c) of the transitional separation bubble

| | | a | b | c | d | e | f | g | h | i |
|---|---|---|---|---|---|---|---|---|---|---|
| $Re_c$=77k | upper | | 0.32 | 0.35 | 0.42 | 0.47 | 0.60 | 0.65 | | |
| | lower | 0.47 | | | | | | | 0.32 | 0.49 |
| $Re_c$=85k | upper | | 0.25 | 0.19 | 0.39 | 0.48 | 0.60 | 0.67 | | |
| | lower | 0.45 | | | | | | | 0.27 | 0.48 |

a)
θ = 0.32°
pitch up
h=-1.65mm
heave up

b)
θ = 7.01°
~ max pitch
h=2.05mm
heave up

c)
θ=6.02°
pitch down
h=2.63mm
~ max heave

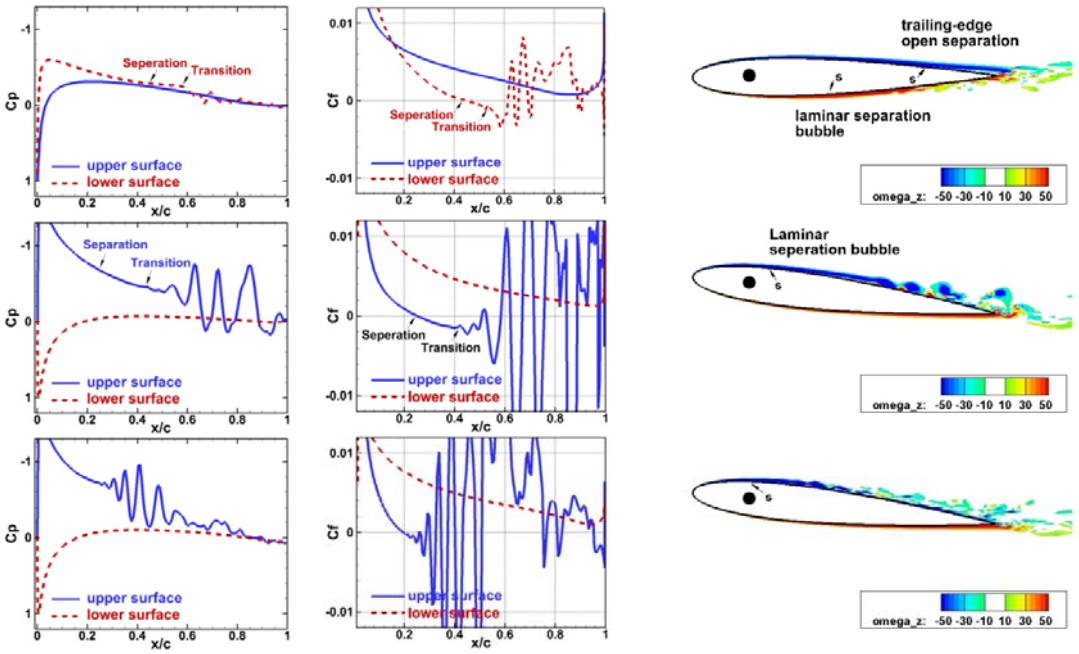


Figure 8. 3D LES computed instantaneous surface pressure coefficients, friction coefficients and non-dimensional spanwise vorticity ($\omega_z$) distributions on the mid-span of the 2DOF pitch-heave NACA 0012 wing during one LCO cycle at $U_\infty$ = 8.25 m/s, $Re_c$ = 85,000. Continued on next page.

d)
θ=1.48°
pitch down
h=1.94mm
heave down

e)
θ = 0.44°
pitch down
h=1.35mm
heave down

f)
θ =-2.33°
pitch down
h=0.65mm
heave down

g)
θ =-3.22°
pitch down
h=0.28mm
heave down

h)
θ =-6.96°
~ max pitch
h=-2.05mm
heave down

i)
θ = 0.25°
pitch up
h=-1.36mm
heave up

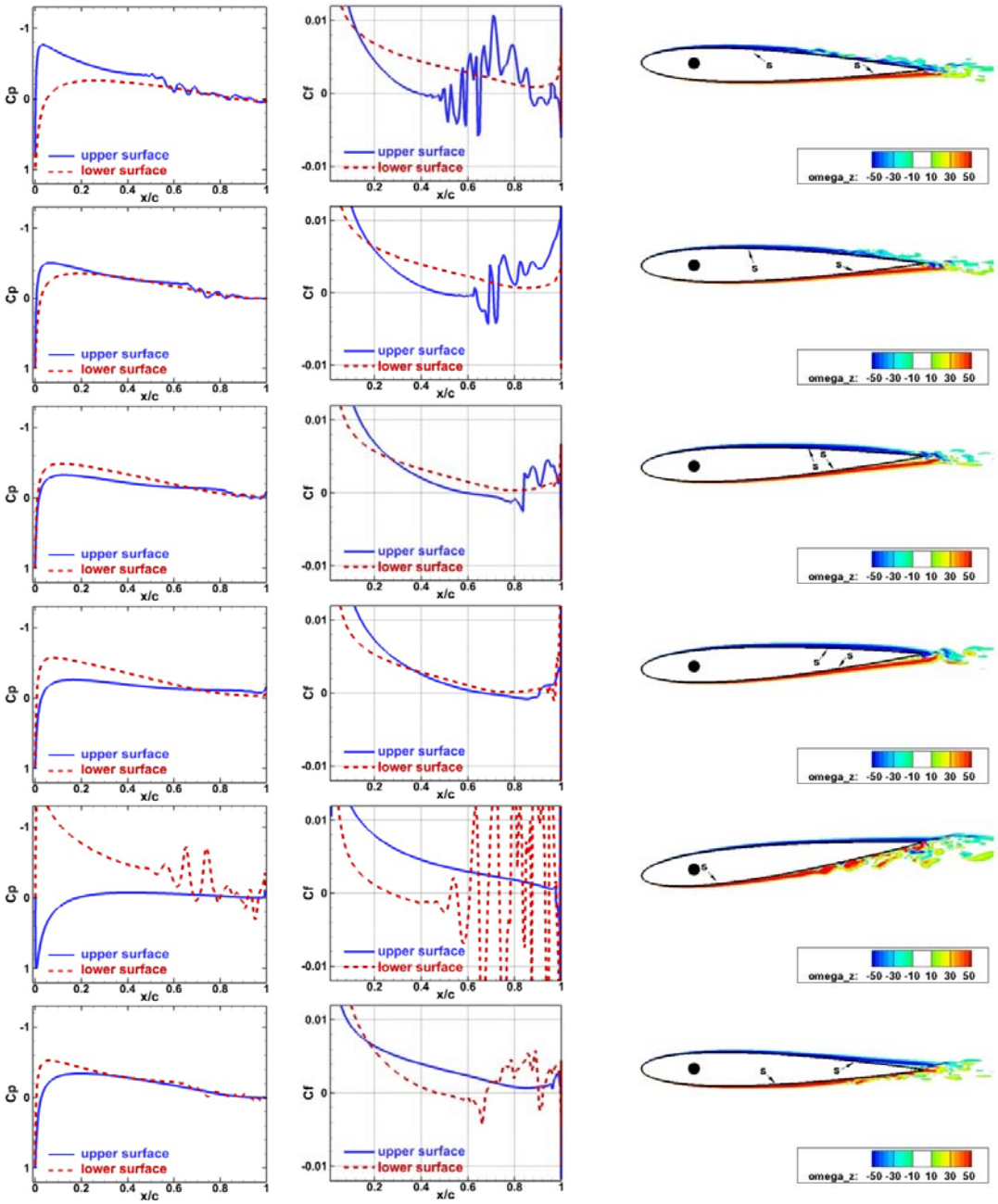


Figure 8. For caption see previous page.